JOURNAL OF AIRCRAFT
Vol. 31, No. 4, July–Aug. 1994

Flowfield Study of a Close-Coupled Canard Configuration

Richard M. Howard* and John F. O'Leary†
Naval Postgraduate School, Monterey, California 93943

A wind-tunnel study was completed examining the flowfield behavior of the canard-vortex/wing-vortex interaction for a close-coupled canard configuration in the post-stall regime. Three cross-planes were mapped in the lee flowfield using a five-hole pressure probe. The mappings traced the canard and wing vortices as they moved downstream, and gave clear evidence that the canard vortex provided the mechanism for flow reattachment over the inboard wing section. The previously separated flow became a coherent wing leading-edge vortex under the canard vortex influence. A tertiary vortex at the canard-fuselage juncture was revealed; this vortex may have an impact upon the resulting flow, and would not be evident in studies of bodiless wings with canards. Surface flow visualization aided in revealing the effects of the post-stall behavior.

Introduction

THE maintenance of air superiority in the future will depend upon an ability to perform rapid transient maneuvers at high angles of attack, often into the post-stall flight regime. The advent of reliable, highly maneuverable all-aspect missiles has brought a quick-kill capability to any air engagement. On the defensive, an aircraft must possess very high speeds and turn rates for intercept avoidance; on the offensive, the aircraft must possess a rapid point-and-shoot capability, and be able to maintain a turn rate margin over his adversary. Maximum sustained turn rates can no longer be increased by conventional means.[1] The longer a turn lasts, the more time an opponent has to set up an attack. For increased survivability in future air combat situations, agility will be required to enable the aircraft to point at an enemy quickly, to continue pointing or maneuvering over prolonged periods of time, and to accelerate rapidly to regain maneuvering speed or for pursuit.[2]

Supermaneuverability has become a topic of increased interest in the popular press[3–6] and in the aerospace professional community.[7–9] Studies continue to develop a set of metrics or parameters by which the performance capability of new fighters can be compared. This new class of metrics is generally distinguished by performing a change in attitude or maneuver in a minimum time, or by holding a flight condition for a specified time interval. A new way of defining flight maneuvers has arrived.

With the advent of highly maneuverable aircraft, a resurgence of interest is taking place in the favorable interaction between a close-coupled canard and a highly swept or delta wing for enhanced lift. Many new fighter aircraft designs, including the Israeli Lavi, the Swedish Gripen, the French Rafale, the French Mirage 3, and the European Fighter Aircraft (EFA), all employ a variation of such a configuration. An exception is the X-31, which uses a long-coupled canard for the purpose of pitch recovery at high angles of attack rather than for enhanced lift.[10]

Received June 8, 1993; presented as Paper 93-3499 at the AIAA Applied Aerodynamics Conference, Monterey, CA, Aug. 9–11, 1993; revision received Oct. 18, 1993; accepted for publication Oct. 18, 1993.

*Associate Professor, Department of Aeronautics and Astronautics, Code AA/Ho. Senior Member AIAA.

†Graduate Student, Aeronautical Engineering, Captain, U.S. Marine Corps; currently Avionics System Project Officer, Naval Air Systems Command, AIR-546E3, Arlington, VA 22203.

Previous Work

The SAAB Viggen aircraft is usually credited with being the first successful operational close-coupled canard configuration.[11] Behrbohm[12] described the aerodynamic gains accomplished with that aircraft. Lift on final approach was increased by 65% over the pure delta wing, although wing loadings were almost identical. The enhancement was due not only to the favorable canard/wing interaction, but also to the trim requirements of the two aircraft: the canard, providing high lift forward of the center of gravity, demands a trimming moment brought about by a positive (trailing-edge-down) wing elevon deflection. This deflection also increases the wing lift. On the other hand, the delta wing used alone must trim with up-elevon deflection, which reduces the overall lift.

Lacey[11] performed an extensive study of the close-coupled canard with regard to relative canard size and canard longitudinal and vertical placement for optimum lift enhancement. Canard leading-edge sweep should exceed that of the wing, to provide a strong canard vortex to affect the formation and position of the wing leading-edge vortex at low angles of attack, and, as is indicated in the current study, to reattach the separated wing flow at high angles of attack. Within the limits of the different geometrical constraints of the tested configuration, recommended guidelines for canard size and placement in the current study followed Lacey's results.

Stoll and Koenig[13] found the canard to delay wing leading-edge vortex breakdown; maintenance of the wing vortex raised the maximum lift coefficient from 1.1 to 1.5 at an angle of attack of 33 deg. Er-El and Seginer[14] and Er-El[15] found that for a close-coupled canard, the onset of vortex breakdown was delayed from an angle of attack of 14–24 deg.

Calerese[16] tested a coplanar and a high canard on a generic fuselage model, and found an increase of 12% in the lift-to-drag (L/D) ratio for the high-canard case. Oelker and Hummel[17] presented surface-pressure and flowfield-measurement results for a 60-deg-swept canard/wing configuration. The results, though well described, were limited to the relatively low angle-of-attack case of 8.7 deg.

Erickson et al.[18] studied a coplanar configuration for compressible flows and found results similar to those of other investigators, that the vortex-dominated flow about the canard induced a downwash on the inboard wing section tending to delay wing vortex formation and flow separation. They noted that the flowfield interaction did not exhibit a favorable lift synergism; in fact, the increase in lift was less than that expected from the simple area increase.

An earlier study by the first author and colleague presented the results of varying canard deflection for a close-coupled-canard configuration through the post-stall regime, with the desire to ascertain the effect on optimal lift enhancement.[19]

The overall lift enhancement was greatest in the regime where initial flow separation over the wing took place, where the canard-leading-edge vortex provided the mechanism to energize and reattach the flow. This result reinforced the notion of using a highly swept canard to provide a strong vortex at angles of attack where wing separation had begun, but no strong wing-leading-edge vortex had yet formed. In the region where the wing-leading-edge vortex itself provided a reattaching mechanism, the canard provided an additional, though smaller, enhancement.

For the geometry tested, with a swept wing and a highly swept canard, studies are lacking of flowfield measurements at the angles of attack for which major lift enhancements were found (above 20 deg). In this regime, the flow over the wing alone is generally separated, and the canard vortex plays a major role in providing apparent reattachment. It was desired to conduct wake surveys using a five-hole pressure probe to map out cross-planes of total pressure and velocity vectors, in order to better quantify the mechanisms of the canard-vortex/wing-vortex interaction for enhanced lift. Although measurement limitations were expected in regions of separated and highly vortical flow, it was felt that changes in the flowfield with and without the canard might be clearly identified by this approach.

Experiment

Wind Tunnel and Test Facility

A wind-tunnel study was carried out for high angle-of-attack tests in the low-speed wind tunnel at the Naval Postgraduate School. The wind-tunnel test section is 28 by 45 in. in cross section, with the reflection plane installed. The wind tunnel has a contraction ratio of about 10, and the ambient turbulence intensity of the test dynamic pressure was 0.2%.

A five-hole, prism-head pressure probe was used for the wake surveys. The probe is of the nulling type, where the sensor is physically turned until the pressure differential between the two horizontal ports is zero. The limit of the probe was reached whenever no pressure equalization was possible, due to the locally strong gradients in the vortex core. Calibration limits on pitch angle were ± 40 deg. The probe was extended from a three-dimensional, computer-driven traverse mounted on the top of the wind tunnel. A rotary pressure scanner driven by a personal computer read the pressures. The signals were then multiplexed through an A/D system for recording with the PC. Multiple signals were read and averaged; no unsteady or time-dependent data were recorded.

Model

A close-coupled canard model was designed for experiments in the low-speed wind tunnel, which accommodates half-models with the use of the reflection plane for force and moment measurements. Figure 1 shows a side view of the half-model in the wind tunnel with the probe in place at one of the cross-plane locations. Note that the model rests on a raised platform above the reflection-plane balance used for the lift-and-drag measurements discussed in Ref. 19. The vertical rise was necessary to allow the probe to reach the desired cross-plane position. The model is seen from an upstream position in Fig. 2. The wing has a 50-deg leading-edge sweep and an aspect ratio of 3; the canard has a 60-deg leading-edge sweep and an aspect ratio of 2. The reference area of the wing was taken to the fuselage centerline; that for the canard was taken as the exposed area, because this was the actual area added between tests. The canard-to-wing area ratio is 0.20. The canard was located a distance of 0.20 mean aerodynamic chord (MAC) above the wing chord plane, and the longitudinal distance from the canard exposed root chord at the 40% chord location to the quarter-chord of the MAC was 1.20, nondimensionalized by the wing MAC. The exposed canard root leading edge is 11.2 in. aft of the nose, and the exposed wing leading edge is 21.55 in. aft of the nose. Exposed root and tip chords are 8.0 and 0.8 in. for the canard, and 11.0 and 2.1 in. for the wing, respectively. The NACA 64A008 airfoil was used for both canard and wing sections. The fuselage was rectangular with rounded corners, with an ogive nose. The fuselage was constructed from mahogany and was slightly oversize with relation to the wing to allow for accommodation of the canard-positioning mechanism. The canard and wing were made from mahogany with aluminum cores. The half-model was 36 in. long with a semispan of 12.1 in. A more complete description of the model geometry can be found in Ref. 20.

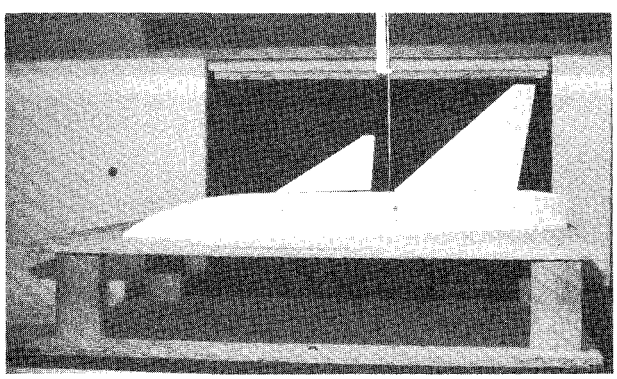

Fig. 1 Wind-tunnel model with probe, side view.

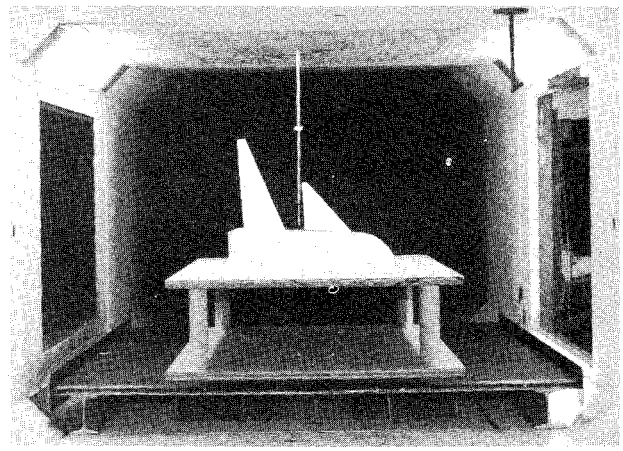

Fig. 2 Wind-tunnel model at 22-deg angle of attack, front view.

Test Conditions

To correlate these results with those of Ref. 19, the experimental conditions were held as identical as possible to the earlier ones. The test-section dynamic pressure was 37.6 lb/ft^2 for an average velocity of 177 ft/s. The Reynolds number based on wing MAC was 9×10^5.

To account for possible tunnel crossflow, probe installation misalignment, and flowfield disturbances caused by the addition of the model platform, an initial run was made without the model installed, to establish baseline freestream-velocity pitch and yaw angles. These measurements were then used as tare values. Measurements were made at three cross-plane locations, as indicated in Fig. 3. The lines shown vertically drawn above the survey-grid dimensions are the cross-planes when looking from above. The survey planes were normal to the freestream flow rather than to the model centerline. Survey grid 1 was 4 by 5 in., grid 2 was 5.5 by 6 in., and grid 3 was 7.5 by 6.5 in., as indicated in Fig. 3. The first two grids were mapped at $\frac{1}{4}$-in. intervals, while the third and larger grid was mapped at $\frac{1}{2}$-in. intervals.

Grid 1 was taken just behind the canard trailing edge in order to capture and define the canard leading-edge vortex. Grid 2 was placed at the midchord location of the wing; grid 3 was placed just behind the trailing edge of the wing. Figure 4 shows a side view of the longitudinal locations of the survey

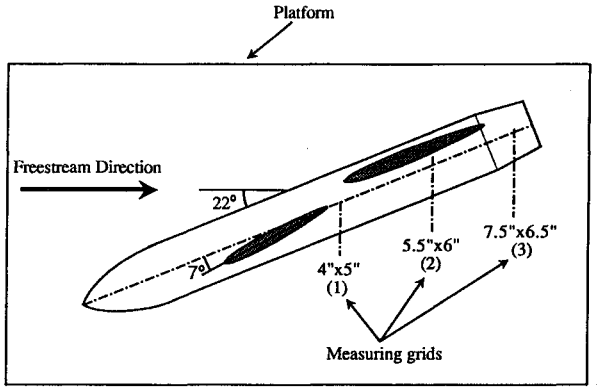

Fig. 3 Sketch showing angle of attack, canard deflection, and measured cross-plane locations and sizes, top view.

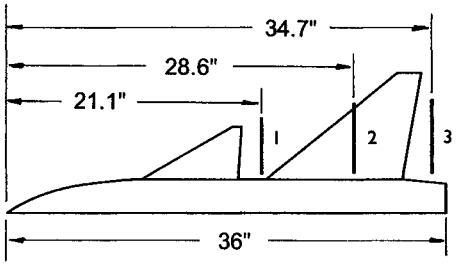

Fig. 4 Sketch showing cross-plane locations, side view; measurements in inches.

planes at their far sides. The location of the corner of each survey plane nearest the model can be described in airplane coordinates x, y, and z, where x is along the centerline (defined aft of the nose); y is spanwise out the wing (measured from the side of the fuselage); and z is below the aircraft centerline. The coordinates are (21.1, 0.8, 0.0) for grid 1; (28.6, 0.8, 0.75) for grid 2; and (34.7, 0.8, 0.3) for grid 3, with all dimensions given in inches. The model was set at 22-deg angle of attack with the canard fixed at a deflection angle of 7 deg, the conditions found in the first study to provide the greatest enhanced lift.

Surface flow-visualization studies were performed to correlate with the earlier force tests and the current flowfield study. In these separate tests, a mixture of black tempera and motor oil was applied with a brush to the model before the tunnel was started. After the oil mixture had stabilized, photographs were taken of the surface flow patterns.

Results

Previous Tests

Figure 5 shows the lift curve from the previous study, comparing the wing-body to the canard-wing-body values of lift coefficient. It should be noted that the additional canard area has been included in the reference area for the canard case; therefore, all enhancement is due to the vortex-vortex interaction, and not to the increased area. Of the cases tested, the greatest increase in lift came in the first post-stall regime at 22-deg angle of attack, where the wing had stalled and no strong wing-leading-edge vortex had yet formed. The optimum canard placement was a deflection of 7 deg (29 deg angle of attack); the lift enhancement was 34%. This condition for model angle of attack and canard deflection was used for the current study. For a more complete discussion of the earlier effort, see Ref. 19.

Current Tests

Shown will be plots of flowfield velocity streamlines, plots of total pressure coefficients (loss in total pressure nondimensionalized by freestream dynamic pressure), and flow-visualization photographs. In the plots, the grids are shown wings-level rather than as measured in the tunnel (with the

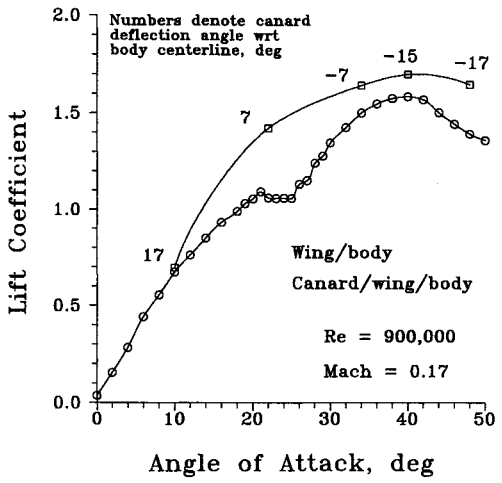

Fig. 5 Comparison of lift with and without canard with optimal canard deflection.[19]

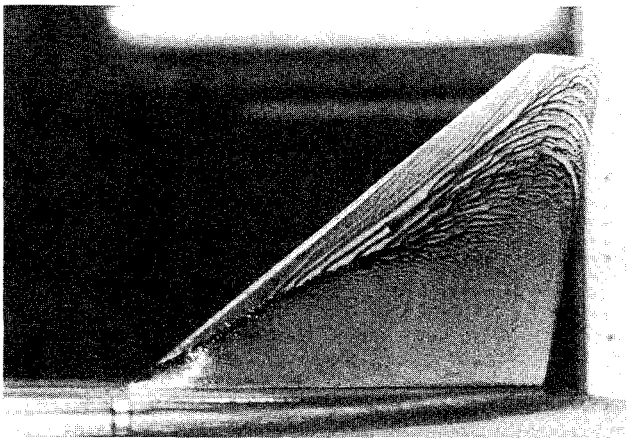

Fig. 6 Surface flow visualization of wing, 22-deg angle of attack, no canard.

wing upward). Part of the model cross section is shown in each plot. The wing-fuselage or canard-fuselage juncture is in the lower right of each figure.

Because of the dynamic nature of flowfields surrounding aerodynamic surfaces at high angles of attack, there were regions in which the capabilities of the probe were exceeded (it could not be nulled). In particular, the probe was unable to make accurate measurements downstream of stalled surfaces or in the core of a strong vortex. The plots have areas where data are not present, and the boundaries of determined data will be noted. Since the probe is unable to distinguish between areas of strong coherent vortical flow or the reversed flow of a stalled surface, the surface flow visualization will be useful in indicating this difference.

Wing-Alone Case

Without the canard, with the wing-body at 22-deg angle of attack, the flow over the main wing was characterized by a large region of reversed flow, indicative of a stalled wing. Figure 6 shows the surface flow visualization. What begins as a secondary-separation line near the wing apex becomes a large separation region over most of the wing. The oil pattern indicates a reversed and spanwise flow moving toward the secondary-separation line. Figure 7 shows the crossflow streamlines from the pressure-probe measurements at grid station 2, at midchord. Graph numbers are in inches measured from the outer grid corner. The black region indicates the area where data were unobtainable due to probe limitations. Although the flow represents a stalled surface, the streamlines indicate a vortex entrainment in the region, and a general clockwise rotation. Figure 8 shows contours of loss of total

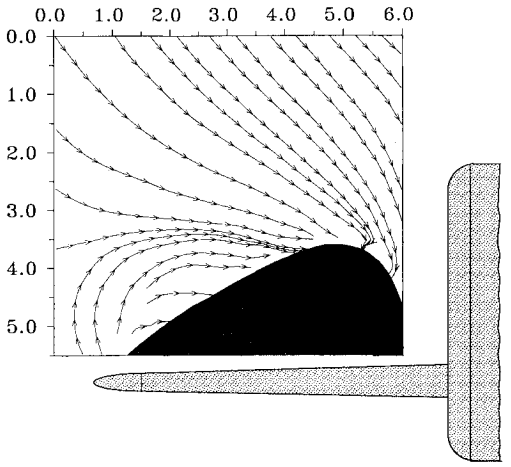

Fig. 7 Cross-plane streamlines, wing midchord (grid 2), no canard; dimensions in inches.

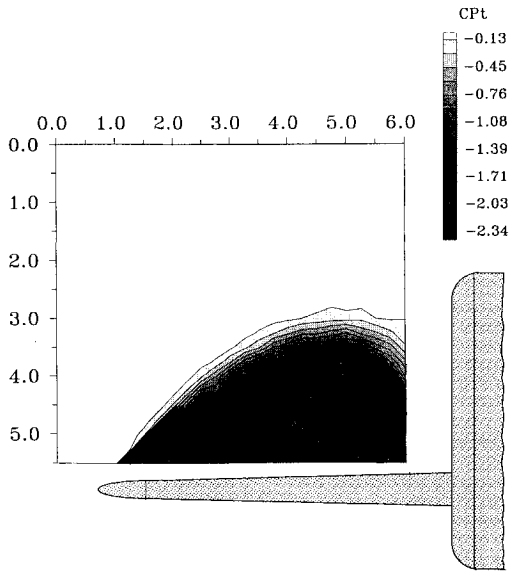

Fig. 8 Cross-plane total-pressure-coefficient loss contours, wing midchord (grid 2), no canard; dimensions in inches.

pressure coefficient. Data were not measurable in the black area, but the contour gradient indicates the rapid change in total pressure at the boundary of the separation region. The size of the separation region clearly supports the flow-visualization photograph in indicating the region to be experiencing separation, rather than a strong coherent vortex.

The crossflow streamlines at the trailing edge of the wing are shown in Fig. 9. The stalled area has greatly increased in size, but the vortex entrainment is still evident. A strong downwash component is evident near the fuselage. Figure 10 shows the total-pressure-coefficient contours. The gradient is more diffuse than at midchord, and the region extends about 60% of the MAC out from the wing surface. The separated region appears to extend spanwise beyond the trailing-edge wingtip, but the extent of the region was not directly measured.

Wing/Canard

The addition of the canard to the model caused large-scale reattachment of the flow over the wing, as expected from the lift results of Fig. 5. Flow visualization over the canard and wing is shown in Fig. 11. At 29-deg angle of attack, the canard produces a strong leading-edge vortex due to the sweep angle of 60 deg. The secondary-separation line is evident from the oil pooling, and the remaining surface is clean. The flow over the wing results in a line of secondary separation parallel to

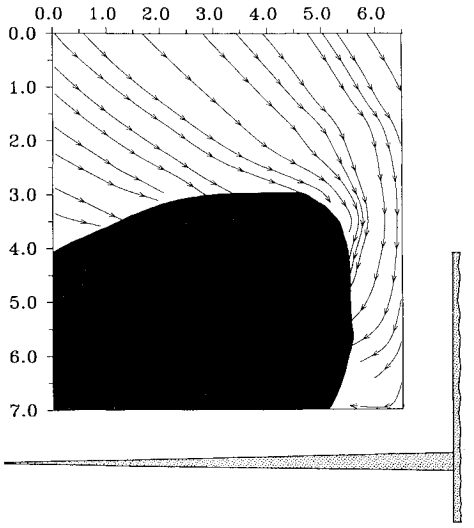

Fig. 9 Cross-plane streamlines, wing trailing edge (grid 3), no canard; dimensions in inches.

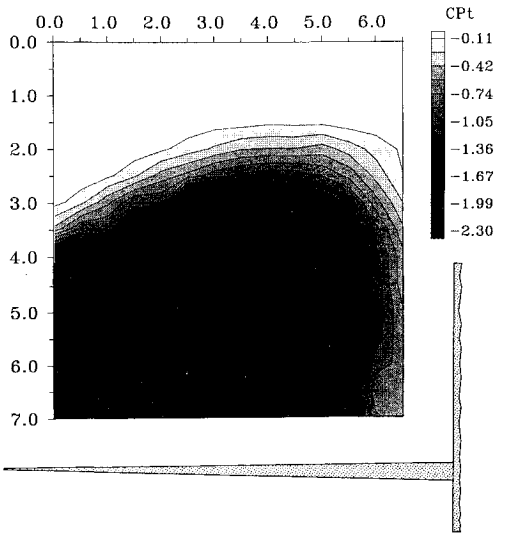

Fig. 10 Total-pressure-coefficient loss contours, wing trailing edge (grid 3), no canard; dimensions in inches.

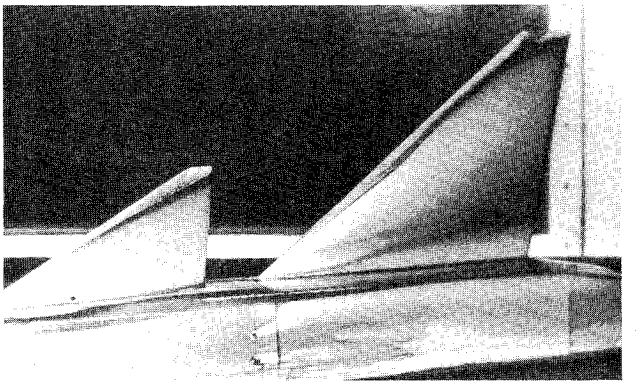

Fig. 11 Surface flow visualization of wing and canard, 22-deg angle of attack, canard deflection 7 deg.

the wing leading edge, and a small amount of pooling can be seen at the trailing edge. Note that, unlike the secondary-separation line apparent on the canard, which is at a sweep angle slightly greater than that of the leading edge, the wing secondary-separation line (and therefore the vortex) is being maintained close to the leading edge. Consistent with the evidence of Ref. 13, the canard vortex acts not only to assist in the formation of a leading-edge vortex over the outer wing

at this high angle of attack, but also to displace it from the location expected on a swept wing at lower angles of attack. The wing is fairly clean of oil with the exception of a wedge starting just aft of the apex and growing as it moves downstream parallel to the fuselage. Not particularly evident in the photograph is the fact that there is a section on the top fuselage surface at the wing/body juncture that is free of oil. The wedge of oil on the lower wing and the clean fuselage area are likely due to the formation of a secondary vortex, as will be shown in the following flowfield plots.

The clockwise action of the strong canard leading-edge vortex is indicated in Fig. 12, with significant changes in the flow direction at (1.0,2.0) in the horizontal (spanwise) and vertical dimensions, respectively, above the canard wingtip. The classical secondary vortex, forming under the primary vortex near the wingtip, is indicated by the streamlines there. The formation of a tertiary vortex near the canard-fuselage juncture is evident in the lower right corner of the grid. The action of this vortex is counterclockwise. It appears to have formed as a result of the interaction of the primary canard vortex with the flow in the juncture of the canard and fuselage; a vortex from the model forebody would be expected to have a clockwise rotation, like that of the canard vortex.

The primary and tertiary vortices are more clearly visible in the pressure contours of Fig. 13. Oddly, the secondary vortex could not be resolved in the pressure plots; see Ref. 20 for the velocity-vector plots that also indicate the existence of the secondary canard vortex. The black area represents the undetermined region. The contour gradients indicate the vortex boundary, with the upper-half of the tertiary vortex captured in the lower right grid. The canard leading-edge vortex has completely and cleanly separated from the wing, as correlates with the flow-visualization photograph.

The following figures show the cross-plane at grid 2, the midchord location. Figure 14 shows the cross-plane streamlines; the separated region on the wing surface has been greatly reduced by the action of the canard vortex, which shows up in the upper portion of the grid. A strong downwash is induced by the canard vortex, which energizes the wing flowfield. In the area of (5.0,4.5), the downwash component is up to 65% of the total freestream velocity. The figure indicates strong rotational behavior, with a saddle point in the outer flow at (2.0,2.0). The energizing of the wing leading-edge vortex over the outer wing section and the reattached flow over the inboard section leads to a level of enhanced lift much greater than that due to the added canard area.

Figure 15 shows a close-up of the wing-surface flow visualization at the test angle of attack. The wedge of oil slightly away from the fuselage is probably a result of the impact of this large downwash component on the wing surface and the action of the tertiary juncture vortex. The region adjoining

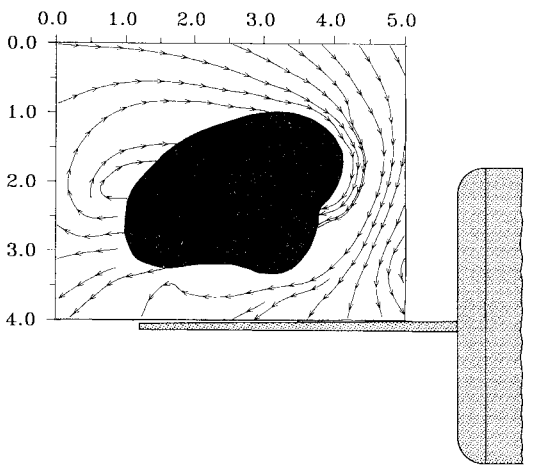

Fig. 12 Cross-plane streamlines, canard trailing edge (grid 1); dimensions in inches.

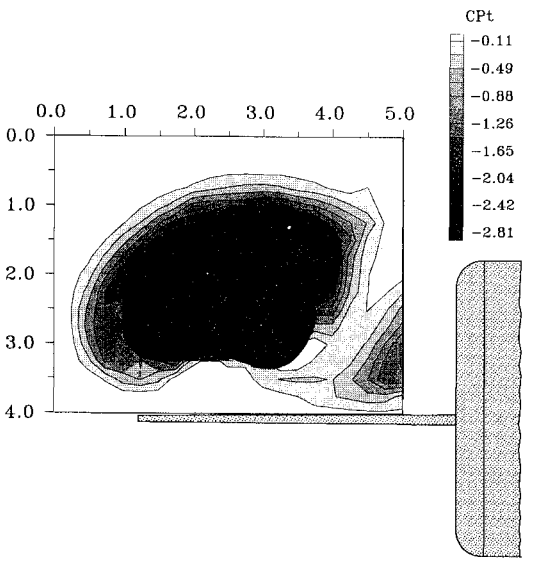

Fig. 13 Total-pressure-coefficient loss contours, canard trailing edge (grid 1); dimensions in inches.

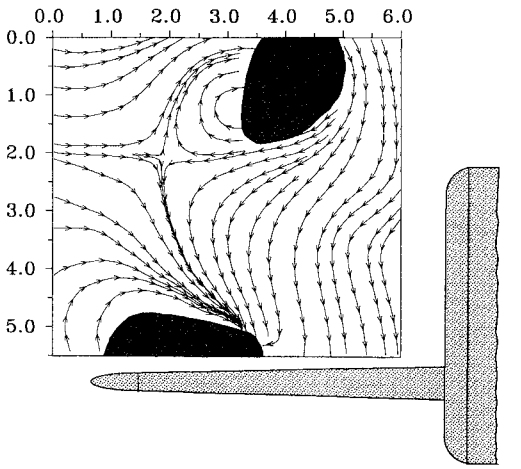

Fig. 14 Cross-plane streamlines, wing midchord (grid 2); dimensions in inches.

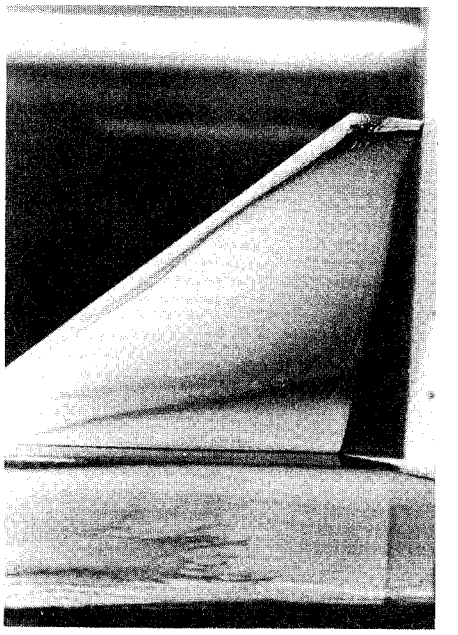

Fig. 15 Surface flow visualization of wing under influence of canard vortex, 22-deg angle of attack.

the wing is not stalled separated flow, as was seen for the wing-alone case, but is the reformation of the coherent wing leading-edge vortex. The flow over the mid to lower wing has reattached.

The total-pressure-loss plot in Fig. 16 captures not only the canard and wing leading-edge vortices, but also the tertiary vortex of opposite rotation noted in the canard plots. This vortex, although weaker than the primary canard vortex, may have a significant impact on the wing surface flow in providing reattachment due to its proximity to the inboard wing section. The oil wedge noted in the flow-visualization photographs may be deposited by the action of the two vortices on either side of it, the strong downwash providing a reattaching region and subsequent oil pooling. If the vortex was initiated by the juncture flow of the canard and fuselage, then studies using a full-span wing and canard may neglect the body's significant influence.

Figures 17 and 18 show plots of cross-plane streamlines and pressure contours at grid 3, at the wing trailing edge. The canard vortex has remained high in the grid, whereas the wing vortex has, of course, followed the leading edge under the influence of the canard vortex and moved to the lower left portion of the grid. The oil pooling in Fig. 14 shows the wing vortex at this point to be interacting with the tip vortex. The

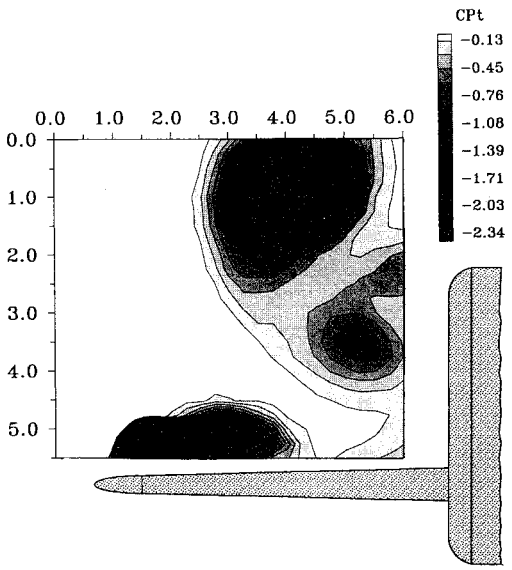

Fig. 16 Total-pressure-coefficient loss contours, wing midchord (grid 2); dimensions in inches.

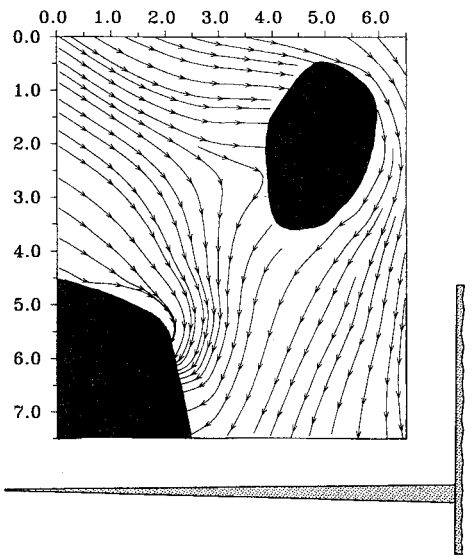

Fig. 17 Cross-plane streamlines, wing trailing edge (grid 3); dimensions in inches.

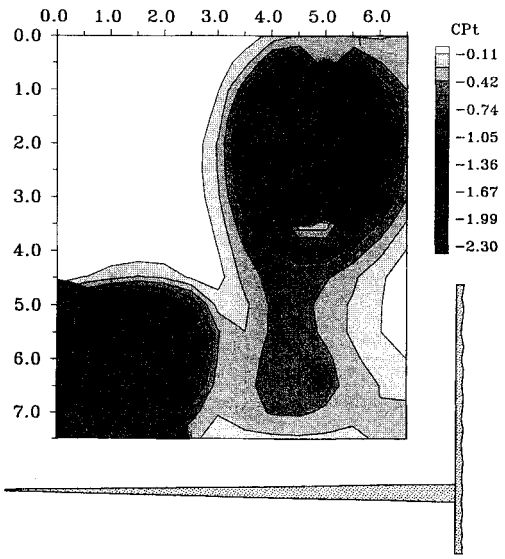

Fig. 18 Total-pressure-coefficient loss contours, wing trailing edge (grid 3); dimensions in inches.

streamlines indicate strong entrainment into the wing leading-edge vortex. As indicated in the flow visualization, the flow over most of the wing has reattached. The total-pressure plot reveals the location of the tertiary vortex, much diffused but still evident, and apparently playing a part in the flow reattachment process. A comparison of Fig. 18 with Fig. 10 shows the significant impact of the canard vortex on wing-flow behavior. Not only can the canard vortex displace the wing vortex outward as shown in earlier studies at lower angles of attack, but it can even provide a reattachment mechanism for the previously separated wing flow, turning a stalled wing into a lifting surface under the influence of a complex vortex system.

Conclusions

Studies of the flowfield behavior of the canard/wing vortex interaction have been extended beyond the 8- to 10-deg angles of attack considered previously, to include an angle of attack of 22 deg, where the first wing stall took place for the tested configuration. Although the extreme flow angles in the lee flowfield prevented a complete pressure mapping of the cross-planes to be carried out, the canard vortex clearly provided the mechanism for massive flow reattachment over the inboard wing section. The flow-visualization helped to indicate that the previously separated (stalled) flow over the wing became a strong coherent leading-edge vortex under the influence of the canard primary and tertiary vortices.

The reattachment can be viewed as a delay in wing vortex breakdown, caused by the high-energy downwash induced by the canard vortex. The inboard wing does accordingly see a reduced angle of attack, and this effect at low angles, where flow separation is minimal, may have led to the reduced lift synergism noted in earlier studies. However, at higher angles (22 deg), the downwash effect of reattaching the separated flow is much more important than the reduction in local angle of attack in promoting enhanced lift.

Acknowledgments

This work was sponsored by AIR-931 of the Naval Air Systems Command under the supervision of Thomas Momiyama and Michael Harris. Funding was provided by the Naval Postgraduate School, Monterey, California, and their support is appreciated. This effort is part of the research initiative supporting NAVAIRs Enhanced Tactical Aircraft Maneuverability program. The authors wish to thank the reviewers and the Associate Editor for their recommendations.

References

[1]Herbst, W. B., "Future Fighter Technologies," *Journal of Aircraft*, Vol. 17, No. 8, 1980, pp. 561–566.

[2]McAtee, T. P., "Agility—Its Nature and Need in the 1990s," *31st Symposium Proceedings of the Society of Experimental Test Pilots* (Beverly Hills, CA), Society of Experimental Pilots, Lancaster, CA, 1987, pp. 54–57.

[3]Cook, W. J., "Turning on a Dime—in Midair," *U.S. News and World Report*, Feb. 20, 1989, pp. 56–58.

[4]Schefter, J., "X-31—How They're Inventing a Radical New Way to Fly," *Popular Science*, Feb. 1989, pp. 58–64.

[5]Scott, W. B., "Air Force, NASA Conduct Tests to Define Fighter Aircraft Agility," *Aviation Week and Space Technology*, Jan. 9, 1989, pp. 45–47.

[6]Scott, W. B., "NASA Adds to Understanding of High Angle of Attack Regime," *Aviation Week and Space Technology*, May 22, 1989, pp. 36–42.

[7]McAtee, T. P., "Agility in Demand," *Aerospace America*, May 1988, pp. 36–38.

[8]Cox, B. W., and Downing, D. R., "Evaluation of Functional Agility Metrics for Fighter Class Aircraft," AIAA Paper 92-4487, Aug. 1992.

[9]Cliff, E. M., and Thompson, B. G., "Aircraft Agility Maneuvers," AIAA Paper 92-4489, Aug. 1992.

[10]Powers, S., and Schellenger, H., "The X-31: High Performance at Low Cost," AIAA Paper 89-2122, July 1989.

[11]Lacey, D. W., "Aerodynamic Characteristics of the Close-Coupled Canard as Applied to Low-to-Moderate Swept Wings, Volume I: General Trends," David W. Taylor Naval Ship Research and Development Center, Rept. DTNSRDC-79/001, Bethesda, MD, Jan. 1979.

[12]Behrbohm, H., "Basic Low Speed Aerodynamics of the Short-Coupled Canard Configuration of Small Aspect Ratio," Svenska Aeroplan Aktiebolag, SAAB TN 60, Linkoping, Sweden, July 1965.

[13]Stoll, F., and Koenig, D. G., "Large-Scale Wind-Tunnel Investigation of a Close-Coupled Canard-Delta-Wing Fighter Model Through High Angles of Attack," AIAA Paper 83-2554, Oct. 1983.

[14]Er-El, J., and Seginer, A., "Vortex Trajectories and Breakdown on Wing-Canard Configurations," *Journal of Aircraft*, Vol. 22, No. 8, 1985, pp. 641–648.

[15]Er-El, J., "Effect of Wing/Canard Interference on the Loading of a Delta Wing," *Journal of Aircraft*, Vol. 25, No. 1, 1988, pp. 18–24.

[16]Calerese, W., "Vortex Interaction Effects on the Lift/Drag Ratio of Close-Coupled Canard Configurations," AIAA Paper 87-1344, June 1987.

[17]Oelker, H.-C., and Hummel, D., "Investigations on the Vorticity Sheets of a Close-Coupled Delta-Canard Configuration," *Journal of Aircraft*, Vol. 26, No. 7, 1989, pp. 657–666.

[18]Erickson, G. E., Schreiner, J. A., and Rogers, L. W., "Canard-Wing Vortex Interactions at Subsonic Through Supersonic Speeds," AIAA Paper 90-2814, Aug. 1990.

[19]Howard, R. M., and Kersh, J. M., Jr., "Effect of Canard Deflection on Enhanced Lift for a Close-Coupled Canard Configuration," AIAA Paper 91-3222, Sept. 1991.

[20]O'Leary, J. F., "Flowfield Study of a Close-Coupled Canard Configuration," M.S. Thesis, Naval Postgraduate School, Monterey, CA, June 1992.